Thin Solid Films 798 (2024) 140381

Contents lists available at ScienceDirect

Thin Solid Films

journal homepage: www.elsevier.com/locate/tsf

Scalable and environmentally friendly production of perovskite manganite thin films for neuromorphic applications

Ville M.M. Paasonen *, Ilari Angervo, Anni Antola, Hannu Huhtinen, Petriina Paturi

Wihuri Physical Laboratory, Department of Physics and Astronomy, The University of Turku, FI-20014, Finland

ARTICLE INFO

Keywords:
Chemical solution deposition
Perovskite manganite
Gadolinium calcium manganite
Resistive switching
Memristor

ABSTRACT

A method of producing high-quality thin films of perovskite manganites utilizing citrate-based aqueous chemical solution deposition is presented. The method is applied to the production of thin films of gadolinium calcium manganite, $Gd_{1-x}Ca_xMnO_3$ (GCMO). The film quality is verified by x-ray diffraction analysis, electron microscopy, and magnetic measurements. Finally, planar memristors are fabricated using GCMO films, demonstrating the material's ability to exhibit resistive switching. This underscores its potential for future memristor technologies.

1. Introduction

Rare earth-doped perovskite manganites [1], functional metal oxides with the chemical formula $R_{1-x}A_xMnO_3$, where R stands for a rare-earth lanthanide and A for an alkaline earth metal and $0 \leq x \leq 1$, have found applications in a broad range of technological fields such as solid-oxide fuel cells [2], spintronics [3] and magnetic refrigeration [4].

In recent breakthroughs, the combination of carefully selected metals like aluminum with specific perovskite manganites, such as $Pr_{1-x}Ca_xMnO_3$ or $La_{1-x}Sr_xMnO_3$ (LSMO), has unveiled an astonishing phenomenon—resistive switching, the hallmark feature of memristors. This remarkable development is poised to revolutionize the landscape of microchip architectures, especially in the realm of neuromorphic computing [5,6]

What is truly exciting is the exceptional promise displayed by perovskite manganite $Gd_{1-x}Ca_xMnO_3$ (GCMO) in terms of switching behavior. Recent studies have indicated that GCMO boasts a distinct advantage—a significantly larger difference in resistance between its low and high resistance states [7,8]. Moreover, the behavior of GCMO-based memristors has been meticulously explored through cutting-edge numerical modeling techniques [9].

Traditionally, the production of perovskite manganite thin films has relied on pulsed laser deposition (PLD). This advanced technique utilizes high-intensity, short-wavelength laser pulses to ablate metal oxide targets, enabling the deposition of material, essentially layer by layer, with unparalleled crystalline quality, uniformity, and surface smoothness [10]. While PLD-produced films are exceptional in quality, it is worth noting that this process can be expensive, inefficient, and challenging to scale. However, even in the face of these challenges, the production and integration of GCMO thin films into various memristor structures have shown immense potential as a groundbreaking technology of the future [7,11,12].

Chemical solution deposition (CSD) is a well-established method of producing many classes of functional oxide thin films on an industrial scale [13,14]. In CSD, a precursor solution containing the target metals in the desired stoichiometric ratio is synthesized. Usually, transition metals and lanthanides are present as coordination complexes to ensure sufficiently high solubility and stability. The precursor is then coated on a substrate (in the case of thin films) by, e.g., spin coating or inkjet printing, heat treated to pyrolyze the ligands and other anions, and annealed to allow the oxide to crystallize. While the quality of the films prepared by CSD methods is generally not quite as good as that of films prepared using PLD, a well-designed CSD protocol can produce epitaxial films with surface smoothness sufficient for microelectronics manufacturing. In particular, CSD methods based on aqueous precursor solutions are attractive to the industry as an environmentally friendly and cost-effective method.

There are reports of perovskite manganite thin films of various compositions produced using CSD in the literature, but they either involve highly toxic and often expensive organometallic precursors and organic solvents [15], or acetate-based precursors [16–20]. The latter have low concentrations, requiring multiple coats to achieve a reasonable film thickness, and poor wetting properties on certain substrates, such as $SrTiO_3$ (STO), resulting in uneven films [14]. There has also been a report of a polymer-assisted approach based on ethylenediaminetetraacetic acid [21], a compound whose manufacturing incurs a significant environmental impact. These issues are resolved by opting

* Correspondence to: COMSOL G.K., 1-10-2-904/905 Kanda Ogawamachi, Chiyoda-ku, Tokyo 101-0052, Japan.
E-mail address: ville.paasonen@comsol.com (V.M.M. Paasonen).

https://doi.org/10.1016/j.tsf.2024.140381
Received 1 November 2023; Received in revised form 22 April 2024; Accepted 10 May 2024
Available online 14 May 2024

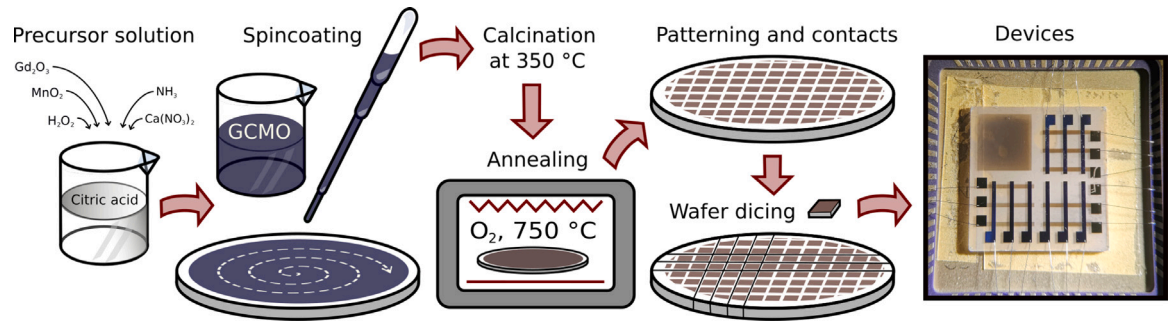

Fig. 1. Schematic depiction of the full manufacturing process of GCMO thin film devices, focusing on the preparation of the GCMO thin films by aqueous chemical solution deposition. The prepared GCMO films can be harnessed across a wide range of future memristor applications, capitalizing on their inherent resistive switching abilities.

for an approach based on aqueous complexes and using a cheap and environmentally friendly chelating agent with good wetting properties. Citric acid is a well-known choice, as it is able to chelate to most transition metals fairly strongly and, owing to its three carboxyl groups and a hydroxy group, it has excellent solubility in water and wetting properties [14]. Furthermore, as a triprotic acid, its coordination behavior can be tuned by adjusting the pH of the solution. However, such a citrate-based aqueous CSD approach for preparing perovskite manganites has not yet been reported in the literature.

In this paper, we present an aqueous citrate-based CSD process to produce perovskite manganite thin films in an industrially scalable and environmentally friendly fashion [8,22]. We apply the process to the synthesis of thin films of GCMO at a range of different values of the stoichiometric ratio x. To demonstrate that the microscopic quality of the films parallels that of GCMO thin films prepared using PLD, we perform X-ray diffraction (XRD) analysis and magnetic measurements. Further, we demonstrate that with only one coat, sufficient film thickness and smoothness for photolithography is attained, thus making microelectronics manufacture possible. Lastly, we use a GCMO film prepared using CSD reported herein to construct a planar memristor, and show that the memristive properties of the film are comparable with PLD films.

A schematic illustration of the full manufacturing process of GCMO thin film devices is shown in Fig. 1, with emphasis on the aqueous CSD-based preparation of the GCMO thin films, which is the main subject of the present paper. It should be noted that in our specific experimental setup, pre-diced substrates were utilized, eliminating the need for wafer dicing in our manufacturing process. Therefore, the intricacies of the wafer dicing technique are not discussed in this work. The depiction of wafer dicing in the schematic serves as a suggestion for potential larger-scale applications of the presented CSD-based process.

2. Experimental

2.1. Materials and reagents

The following materials and reagents were used in the synthesis of the precursor solution: citric acid monohydrate (VWR Chemicals), gadolinium (III) oxide (99.9%, Acros Organics), manganese (IV) oxide (99.9%, 325 mesh powder, Alfa Aesar), hydrogen peroxide (33% aqueous solution, VWR Chemicals), ammonia (min. 25% aqueous solution, VWR Chemicals), and calcium nitrate tetrahydrate (99%, Aldrich).

2.2. Precursor solution

In this section we describe the synthetic procedure for preparing n moles of precursor solution that can be used to produce films with molar ratio x. A schematic representation of the procedure described in this section is shown in Fig. 2.

An aqueous solution of gadolinium citrate was prepared by dissolving $\frac{1-x}{2}n$ moles of gadolinium (III) oxide in a hot (80 °C) ~ 1M solution of $(2-x)n$ moles of citric acid. At least a 3-fold molar excess of citric acid was required for this reaction to proceed. This guarantees a sufficiently low pH of around 3 required for the dissolution. The resulting clear and colorless solution was allowed to cool, diluted to a concentration of ~0.1M, and n moles of manganese (IV) oxide was added so that a 1:1 molar ratio of metal to citrate was obtained. Hydrogen peroxide was added drop-wise, resulting in the reduction and dissolution of the manganese into solution according to the following reaction equation,

$$MnO_2\ (s) + H_2O_2\ (aq) + H_3Cit\ (aq) \xrightarrow{pH\leq 5} Mn(HCit)\ (aq) + O_2\ (g) + 2H_2O\ (l).$$

Due to the competing catalytic breakdown of hydrogen peroxide taking place, a roughly 1.3-fold molar excess of peroxide versus manganese was needed for the complete conversion of all Mn^{4+} to Mn^{2+} (Using less resulted in a cloudy solution due to the presence of unreacted manganese(IV) oxide, whereas using more resulted in excessive bubbling of oxygen due to the breakdown of unreacted hydrogen peroxide in the following step). In this reaction, hydrogen peroxide is acting as a reducing agent due to the low pH. After leaving the solution to react overnight, a clear solution whose color depended on the gadolinium concentration (pale yellow at low Gd concentrations, orange-red at higher Gd concentrations) was obtained.

The pH of the solution was increased to 8 using ~$1.3n$ moles of ammonia, facilitating the oxidation of manganese(II) to manganese(III) by ambient oxygen and the complete deprotonation of the citric acid according to the following reaction equation

$$2Mn(HCit)\ (aq) + \frac{1}{2}O_2\ (aq) \xrightarrow{pH\geq 8} 2[Mn\ (Cit)]\ (aq) + H_2O\ (l),$$

thus yielding a stable solution of the 1:1 citrato complexes of Mn^{3+} and Gd^{3+}. It is also possible that some of the excess hydrogen peroxide partook in the reaction as an oxidizing agent at the lower pH. The solution remained clear but the color deepened significantly. While colorless on its own, gadolinium strongly affected the color of the solution in the presence of manganese, which suggests the formation of cluster complexes. It should also be noted that there are reports of citric acid deprotonating a fourth time at the hydroxy group under similar circumstances [23]. In the present case, occurrence of the Cit^{4-} ion may enable coordination of NH_4^+ or presence of Mn^{4+} centers. The solution was evaporated on a hotplate at 50–60 °C until the desired concentration was reached. Concentrations of up to 1 M of manganese, yielding film thicknesses of over 100 nm in a single coating, were found to be stable over several weeks.

Calcium citrate is poorly soluble in water, so the highly soluble calcium nitrate was used as a source of calcium. A concentrated aqueous solution of calcium nitrate was prepared separately, and xn moles of it was added to the Gd-Mn precursor solution described above yielding the desired stoichiometry of the metals immediately before coating to avoid crystallization of calcium citrate. The main limitation to the film quality achievable by this method arises from large concentrations of calcium nitrate needed to reach high x. The violent thermal decomposition of the nitrate easily results in the blistering of the film surface.

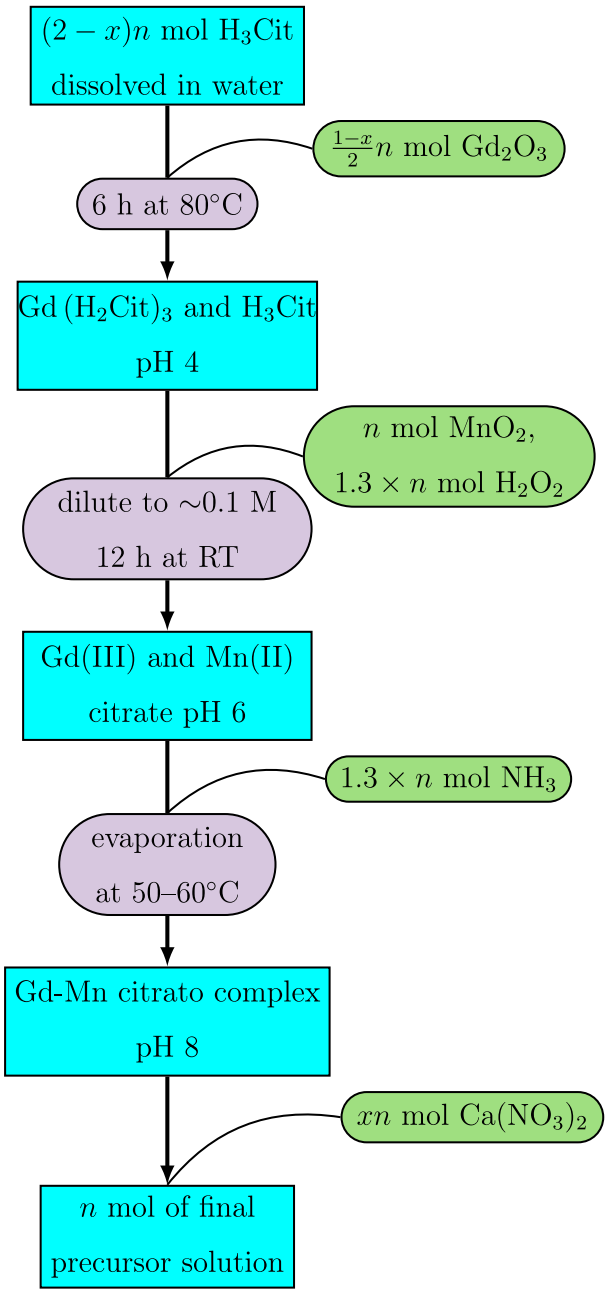

Fig. 2. A schematic representation of the synthesis of the precursor solution for GCMO thin films.

To overcome this, at least part of the nitrate could be replaced by acetate or another suitable calcium salt. However, as mentioned in the previous section, using too much acetate will interfere with the wetting properties of the solution, which results in an uneven coating.

By following the above procedure and varying the molar ratio Gd:Mn:Ca, precursor solutions with manganese concentration of 1 M corresponding to GCMO with $x = 0.75$ and $x = 0.95$ were prepared. From these solutions, a precursor with any intermediate stoichiometry $0.75 \leq x \leq 0.95$ can readily be prepared by simply mixing the two solutions in the appropriate ratio.

2.3. Spin coating, pyrolysis and annealing

Thin films of precursors with varying values of x were prepared by applying a single coat on monocrystalline 5 mm × 5 mm STO (100) substrates provided by Crystal GmbH by spin coating at 5000 rpm, followed by calcination at 350 °C under atmospheric conditions. The temperature was ramped at approximately 0.5 °C/min to minimize damage to the film surface. Finally, the films were annealed at 750 °C for 24 h under an oxygen atmosphere to allow the crystallization of GCMO on the STO surface.

2.4. Etching GCMO

For applications of GCMO in microchip device manufacturing, it is important that we can etch patterns on the films. Here, we discuss wet chemical etching of GCMO thin films as part of the photolithography process. We apply an approach reported to work well for LSMO [24]. In essence, the etchant is based on chloride reducing the manganese to the water-soluble manganese (II) under acidic conditions in the presence of iodide facilitating the reduction of the elemental chlorine formed back to chloride thus providing a way to regulate the speed of the process. We have used the following aqueous etchant composition to etch GCMO thin films for photolithography:

$$[HCl] = 0.12\,M, \quad [KI] = 5\,M, \quad [\text{Ascorbic acid}] = 0.1\,M$$

Ascorbic acid is added to prevent oxidation of iodide which leads to the solution becoming opaque. A 1:1 dilution of the etchant yielded etch times of 1–2 min depending on the film.

We note that the etchant described above is highly selective; while we expect it to etch other manganite perovskites, as only a mild reducing agent it does not damage e.g. metal films ([HCl] too low) or SRO ($SrRuO_3$) films.

2.5. Measuring equipment

Microstructural attributes were characterized with PanAnalytical Empyrean X-ray diffractometer with five-axis goniometer. Diffractometer was utilized with Empyrean Cu LFF HR X-ray tube. The filtered X-ray radiation consists mainly of Cu $K_{\alpha 1}$ and $K_{\alpha 2}$ components. The measurements included θ–2θ scans between 20°–120°, ϕ–ψ, 2θ–ϕ and ω–2θ scans for the GCMO (204) peak ($2\theta = 60.67°$). In addition, the GCMO (224) peak ($2\theta = 71.36°$) was recorded with 2θ–ϕ and ω–2θ measurements.

The surface characterization was accomplished with an Innova atomic force microscope provided by Bruker using contact mode with μmasch tips and an Apreo S high-resolution field emission Scanning Electron Microscope (SEM) provided by Thermo Scientific, and equipped with an energy-dispersive X-ray spectroscopy (EDS) (Oxford Instruments Ultim Max 100) system for compositional analysis. SEM imaging was done with acceleration voltage of 2 kV, while the EDS spectrum was obtained with 10 kV.

The resistive characteristics were measured by connecting the memristor device to a Keithley 2614B SourceMeter, and pulsed voltage sweep sequences of 0 V → +20 V → −20 V → 0 V with 0.1 V steps were performed five times to investigate its resistive switching behavior. Between each voltage step a low reading voltage of 0.4 V was applied as a probe voltage. The pulses had a width of 50 ms.

The temperature dependences of the zero-field-cooled (ZFC) and field-cooled (FC) magnetizations were measured with a Quantum Design SQUID magnetometer between temperatures of 10 and 400 K in 50 mT magnetic field. During the measurements, the magnetic field was oriented along the plane of the film i.e. the GCMO (110) axis.

3. Results and discussion

3.1. Verifications of film quality

Below in Fig. 3 we show SEM images of the $x = 0.75$ (a) and $x = 0.95$ (b) films to demonstrate that, while the film surfaces are not atomically smooth (during pyrolysis, exhaust gases escape from

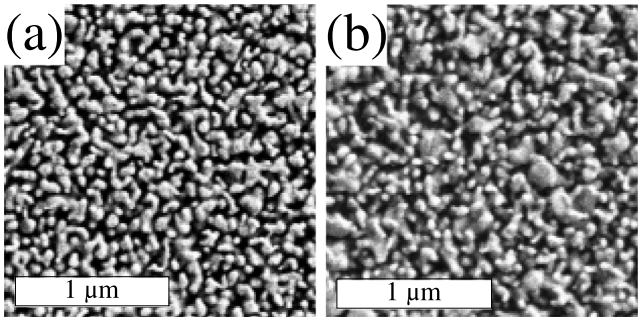

Fig. 3. SEM images of the surface of the GCMO films with $x = 0.75$ (a) and $x = 0.95$ (b) prepared by CSD.

Table 1
Measured stoichiometry (in atomic percent) of the CSD GCMO thin films obtained by EDS compared to the expected stoichiometry for $x = 0.75$ and $x = 0.95$.

	$Gd_{1-x}Ca_xMnO_3$ $x = 0.75$		$Gd_{1-x}Ca_xMnO_3$ $x = 0.95$	
	Theoretical	Measured	Theoretical	Measured
Gd	12.5%	15.3%	2.5%	3.5%
Ca	37.5%	37.6%	47.5%	46.2%
Mn	50.0%	47.1%	50.0%	50.3%

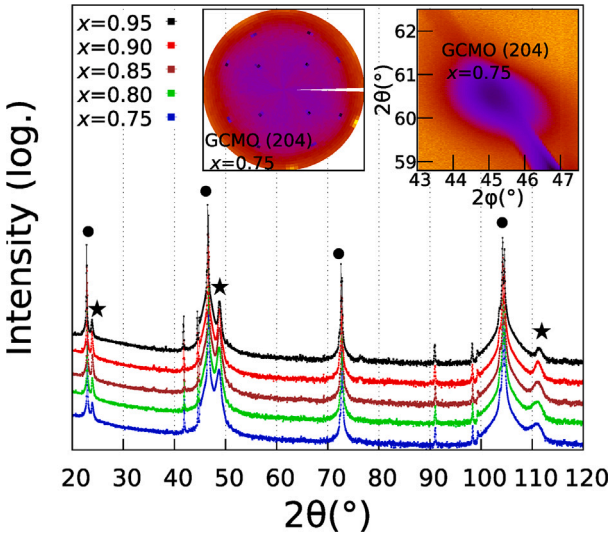

Fig. 4. XRD results demonstrate the c-axis oriented and textured GCMO phase. The main panel presents $\theta - 2\theta$ results with peaks of the GCMO and the STO phase. GCMO $(00l)$ peaks are labeled with ⋆-symbol and substrate peaks with ●-symbol. The insets present Φ–Ψ and 2θ–Φ for the GCMO (204) peak, demonstrating a fully textured phase.

the film, so generally CSD is not a suitable technique for extremely smooth films), it is smooth enough for microelectronics manufacture. Utilizing the EDS feature of the SEM, the stoichiometry of the films was confirmed to be close to the theoretical predictions, as shown in Table 1.

Furthermore, we tested the etching procedure described in the previous section by etching stripes into the $x = 0.75$ film. We were thus able to obtain a rough measurement of the film thickness by measuring the thickness of the stripes using the atomic force microscope: with a single coating of the undiluted precursor, a film thickness of ~100 nm was obtained.

θ–2θ results presented in Fig. 4 show $(00l)$ peaks both from the STO substrate and the GCMO film. Peak identification for GCMO is based on Ref. [25]. GCMO $(00l)$ peaks are identified with ⋆-symbol and respective substrate peaks with ●-symbol. Please note that the indexing of the b and c parameters has been switched for convenience. The pole figure obtained from the GCMO (204) peak is presented in Fig. 4 left inset. The results suggest a fully texturized GCMO phase. This is supported by the detailed 2θ–ϕ scan of the GCMO (204) peak presented in the right inset and additional scans of the GCMO (224) peak, which are not presented here. These results are evidence for a crystallized and textured GCMO phase, which appears similar to that observed in GCMO films on STO substrates prepared using PLD [11,26]. Based on the analysis presented here, there are no differences between the samples.

The magnetic transitions of the spin-coated GCMO thin films with the Ca concentrations of $0.75 \leq x \leq 0.95$ were studied by measuring the zero-field-cooled (ZFC) and field-cooled (FC) magnetizations M in the temperature range of 10–400 K and in 50 mT external magnetic field, as shown in Fig. 5(a) and (b). For $0.75 \leq x \leq 0.85$, it is evident that the FC magnetization experiences an augmentation as the temperature decreases. Conversely, the ZFC curves display a non-monotonic pattern with a peak occurring below the Néel temperature T_N. This particular behavior has been documented previously and can be understood through the ferromagnetic cluster model [27,28]. According to this model, the presence of a minor peak in the ZFC curve below T_N can be ascribed to spin-glass behavior arising from the interplay of ferromagnetic (FM) and antiferromagnetic (AFM) interactions [29,30]. As x exceeds 0.9, the FC magnetization curve demonstrates a more pronounced FM-like behavior, significantly increasing in magnitude. In contrast, the ZFC magnetization exhibits a substantial hump just below T_N. These phenomena can be interpreted as a competition between the random local magnetization orientations of the clusters under the influence of an applied magnetic field, as previously expounded in detail [11].

As illustrated in the inset of Fig. 5(b), the magnetic ordering temperatures, determined from the peak in the ZFC curve below T_N associated with the AFM transition in the range $0.75 \leq x \leq 0.85$ and the spin-glass or cluster-glass type transition in the range $0.90 \leq x \leq 0.95$, exhibit a nearly linear increase from approximately 95 K to around 105 K with increasing Ca concentration. According to the magnetic phase diagrams [11,31], these ordering temperatures align closely with the findings for ceramic bulk GCMO and GCMO thin films produced by PLD with the same Ca doping concentrations. It is noteworthy, however, that the paramagnetic upturn in the magnetization temperature curves at low temperatures for $x \leq 0.85$ appears to be more pronounced in spin-coated thin films than in films prepared by PLD.

3.2. Building a planar memristor

To verify that the GCMO films prepared using CSD as described above exhibit resistive switching, a crude planar memristor was built on the GCMO film with $x = 0.85$ by depositing spots of gold thin film to be used as the cathode (it has been shown that gold makes an ohmic contact with GCMO and thus does not influence memristive properties [7]). Aluminum wire contacts were made using a wire bonder to the gold cathode (this is also an ohmic contact), and directly to the GCMO film to provide the anode. It is this interface between the aluminum and the GCMO that has been shown to function as a memristor.

Fig. 6(a) presents hysteretic resistance states for a GCMO-based planar memristor. The results, as described in Section 2.5, were obtained with a voltage sweep sequence of 0 V → +20 V → −20 V → 0 V with 0.1 V steps. The blue curve refers to resistance value obtained with the corresponding current voltage measurements (i.e. IV measurements).

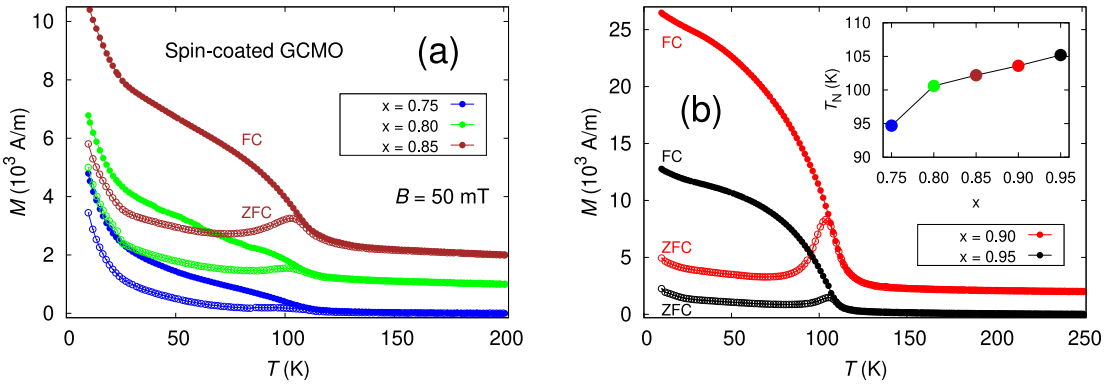

Fig. 5. Temperature dependence of the ZFC (lower curves with open circles) and FC (upper curves with filled circles) magnetizations M originally measured in 50 mT field at temperatures from 10 to 400 K for spin-coated GCMO thin films with different calcium concentrations $0.75 \leq x \leq 0.95$. In the inset of (b) is shown the evolution of T_N with increasing x. Note that in both (a) and (b) the $M(T)$ curves are shifted at high temperatures to facilitate easy comparison of the differences in the vicinity of the phase transition temperature.

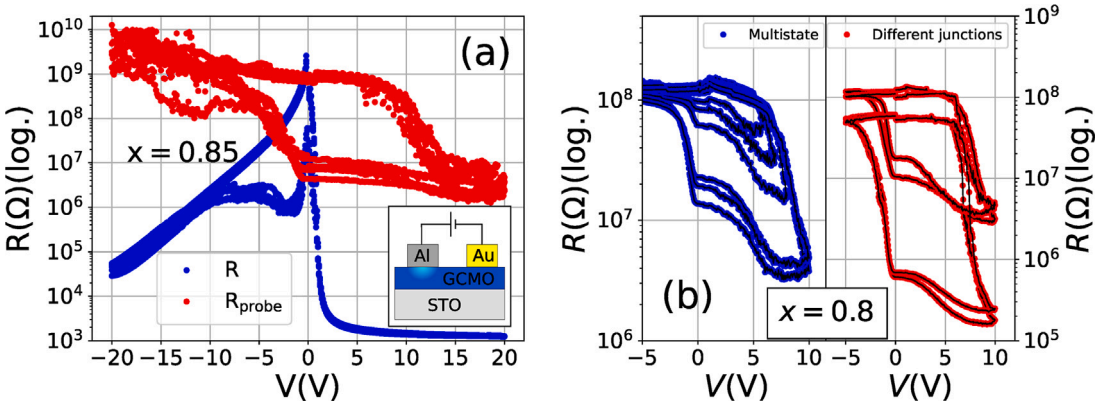

Fig. 6. The IV-plot of 5 pulsed sweeps performed on a memristor constructed using a GCMO film prepared using CSD as described above, with $x = 0.85$ (a). Both the 'write' (blue) and the 'read' (red) pulse plots are shown. It can be clearly seen that the sample exhibits resistive switching. The inset shows a schematic of the device set-up in which the Al/GCMO interface acts as a switching component. The IV-plot of pulsed sweeps performed on four different junctions prepared using a GCMO thin film with $x = 0.8$ (b).

Between each 0.1 V voltage step in the measurement sequence the memristor was probed with a low reading voltage of 0.4 V. These results are depicted by the red curve in Fig. 6(a). it can clearly be seen from the hysteretic (multivalued) nature of the resistance and the probed resistance as a function of voltage that the state of the sample depends on the history of the voltages it has been subjected to in a robust fashion, that is, this sample exhibits resistive switching.

Applying a positive voltage sequence sets the device from a stable high resistance state to a stable low resistance state, whereas applying a voltage sequence with reversed polarity switches the sample into a high resistance state. In perovskite manganite-based systems the phenomenon is usually argued to originate from the movement of oxygen vacancies at the active electrode interface [32–37]. In the present case, the memristor device is created by the interface between the aluminum electrode and GCMO. Our previous work has already demonstrated the resistive switching phenomenon in GCMO films prepared using PLD [7]. The earlier work has also demonstrated optimal resistive switching performance at the vicinity of $x = 0.85$, with approximately two orders of magnitude difference between the low and high resistance states in reproducible resistive switching. The same switching ratio is indeed confirmed here as depicted by the probed resistance levels in Fig. 6. The probed states also show only minor deviation between stable resistance states. Furthermore, Fig. 6(b) shows the analog control of the low resistance states, achieved by applying IV measurements with varying positive sweep amplitude, and similar resistive switching performance in four different junctions. Hence it can be concluded that GCMO-based devices, prepared by CSD, can be harnessed as memristors.

4. Conclusions

In this paper, we have reported an environmentally friendly and industrially scalable pathway to produce perovskite manganite thin films. Our approach is based on an aqueous citrate precursor system, and it was applied to producing thin films of the perovskite manganite GCMO. The obtained films were epitaxial and fully textured, and their magnetic properties were comparable to films prepared by PLD. Furthermore, a planar memristor constructed on the film exhibited resistive switching, so the CSD-based GCMO films show promise as a material for memristive networks applied to neuromorphic computing.

While the method developed here was applied to the production of GCMO thin films, we are confident that the pathway is applicable to any perovskite manganite, by replacing gadolinium oxide with the oxide or hydroxide of the desired lanthanide, and calcium nitrate by the

nitrate or other water-soluble salt of the desired earth alkaline metal. Furthermore, we used the precursor solution for preparing thin films of GCMO by means of spin coating, but other possibilities exist. For instance, the dried precursor gel could be pyrolyzed in bulk to produce perovskite manganite nanoparticles.

As a continuation of this study, we intend to explore using GCMO thin films prepared by CSD to manufacture a network of capacitive instead of planar memristors as a proof-of-concept economical and environmentally friendly hardware-based neural network. While not aligned with the aims of the present study, another intriguing future prospect of this study would be elucidating the structure of the coordination sphere of manganese and gadolinium in the precursor solution spectroscopically. This would likely shed light on the dependence of the solution color on gadolinium concentration as well as the possible presence of quadruply deprotonated citrate.

CRediT authorship contribution statement

Ville M.M. Paasonen: Writing – review & editing, Writing – original draft, Validation, Methodology, Investigation, Conceptualization. **Ilari Angervo:** Writing – review & editing, Writing – original draft, Visualization, Validation, Formal analysis, Data curation. **Anni Antola:** Visualization, Formal analysis. **Hannu Huhtinen:** Writing – review & editing, Writing – original draft, Validation, Supervision, Formal analysis. **Petriina Paturi:** Supervision, Resources, Project administration, Funding acquisition, Conceptualization.

Declaration of competing interest

The authors declare that they have no known competing financial interests or personal relationships that could have appeared to influence the work reported in this paper.

Data availability

Data will be made available on request.

Acknowledgments

The Jenny and Antti Wihuri Foundation, Finland is acknowledged for financial support.

References

[1] W. Xia, Z. Pei, K. Leng, X. Zhu, Research progress in rare earth-doped perovskite manganite oxide nanostructures, Nanoscale Res. Lett. 15 (2020) http://dx.doi.org/10.1186/s11671-019-3243-0.

[2] S.P. Jiang, Development of lanthanum strontium manganite perovskite cathode materials of solid oxide fuel cells: a review, J. Mater. Sci. 43 (2008) 6799, http://dx.doi.org/10.1007/s10853-008-2966-6.

[3] N.V. Volkov, Spintronics: manganite-based magnetic tunnel structures, Phys.-Usp. 55 (2012) 250–269, http://dx.doi.org/10.3367/ufne.0182.201203b.0263.

[4] Z. Xie, Z. Zou, B. He, L. Liu, Z. Mao, Research progress of doped manganite materials in magnetic refrigeration, Front. Mater. 8 (2021) http://dx.doi.org/10.3389/fmats.2021.771941.

[5] W. Chen, L. Song, S. Wang, Z. Zhang, G. Wang, G. Hu, S. Gao, Essential characteristics of memristors for neuromorphic computing, Adv. Electron. Mater. 9 (2023) 2200833, http://dx.doi.org/10.1002/aelm.202370012.

[6] D. Ielmini, Z. Wang, Y. Liu, Brain-inspired computing via memory device physics, APL Mater. 9 (2021) 050702, http://dx.doi.org/10.1063/5.0047641.

[7] V. Lähteenlahti, A. Schulman, A. Beiranvand, H. Huhtinen, P. Paturi, Electron doping effect in the resistive switching properties of Al/$Gd_{1-x}Ca_xMnO_3$/Au memristor devices, ACS Appl. Mater. Interfaces 13 (2021) 18365–18371, http://dx.doi.org/10.1016/j.mee.2015.04.043.

[8] P. Paturi, A. Schulman, H. Huhtinen, V. Lähteenlahti, A. Beiranvand, Novel thin film material for memristor, and a memristor comprising such material, Patents FI20205101 (31.1.2020), PCT/FI2021/050057 (29.1.2021), TW110103063 (27.1.2021), 2020.

[9] E. Miranda, V. Lähteenlahti, H. Huhtinen, A. Schulman, P. Paturi, Compact modeling and SPICE simulation of GCMO-based resistive switching devices, IEEE Trans. Nanotechnol. 21 (2022) 285–288, http://dx.doi.org/10.36227/techrxiv.19181678.

[10] D.B. Chrisey, G.K. Hubler, Pulsed Laser Deposition of Thin Films, John Wiley Sons Inc., 1994, http://dx.doi.org/10.1887/0750306076/b1388v3c9.

[11] A. Beiranvand, J. Tikkanen, H. Huhtinen, P. Paturi, Metamagnetic transition and spin memory effect in epitaxial $Gd_{1-x}Ca_xMnO_3$ ($0 \le x \le 1$) thin films, J. Magn. Magn. Mater. 469 (2019) 253–258, http://dx.doi.org/10.1016/j.jmmm.2018.08.002.

[12] A. Schulman, A. Beiranvand, V. Lähteenlahti, H. Huhtinen, P. Paturi, Appearance of glassy ferromagnetic behavior in gcmo thin films: A revised phase diagram, J. Magn. Magn. Mater. 498 (2020) 166149, http://dx.doi.org/10.36227/techrxiv.19181678, 1–6.

[13] R.W. Schwartz, T. Schneller, R. Waser, Chemical solution deposition of electronic oxide films, C. R. Chimie 7 (2004) 433–461, http://dx.doi.org/10.1016/j.crci.2004.01.007.

[14] T. Schneller, R. Waser, M. Kosec, D. Payne, Chemical Solution Deposition of Functional Oxide Thin Films, Springer, Vienna, 2014, http://dx.doi.org/10.1007/978-3-211-99311-8.

[15] K. Tanaka, S. Okamura, T. Shiosaki, Fabrication of perovskite manganite (La, Sr)MnO_3 thin films by chemical solution deposition and their low-field magnetoresistance properties at room temperature, Japan. J. Appl. Phys. 40 (2001) 6821–6824, http://dx.doi.org/10.1143/jjap.40.6821.

[16] P.S. Solanki, R.R. Doshi, U.D. Khachar, R.J. Choudhary, D.G. Kuberkar, Thickness dependent transport and magnetotransport in CSD grown $La_{0.7}Pb_{0.3}MnO_3$ manganite films, Mater. Res. Bull. 46 (2011) 1118–1123, http://dx.doi.org/10.1016/j.materresbull.2011.02.044.

[17] T.M. Tank, C.M. Thaker, R.S. Chhatrala, V. Ganesan, S.P. Sanyal, Enhancement of temperature and field coefficient of resistance in CSD grown nanostructure $La_{0.7}Ca_{0.3}MnO_3$ thin films, J. Nano Res. 24 (2013) 155–162, http://dx.doi.org/10.4028/www.scientific.net/jnanor.24.155.

[18] P.S. Solanki, R.R. Doshi, A. Ravalia, M.J. Keshvani, S. Pandya, V. Ganesan, N.A. Shah, D.G. Kuberkar, Transport studies on $La_{0.8-x}Pr_{0.2}Sr_xMnO_3$ manganite films, Physica B 465 (2015) 71–80, http://dx.doi.org/10.1016/j.physb.2015.02.019.

[19] M. Saito, M. Hagiwara, S. Fujihara, Chemical solution deposition of magnetoelectric ZnO-La_2CoMnO_6 nanocomposite thin films using a single precursor solution, Mater. Chem. Phys. 236 (2019) 121762, http://dx.doi.org/10.1016/j.matchemphys.2019.121762.

[20] D. Venkateshwarlu, H. Dadhich, B. Rajyaguru, S. Hans, M. Ranjan, R. Venkatesh, V. Ganesan, P. Solanki, N. Shah, Semiconducting nature and magnetoresistance behaviour of ZnO/$La_{0.3}Ca_{0.7}MnO_3$/$SrTiO_3$ heterostructures, Mater. Sci. Semicond. Process. 136 (2021) 106154, http://dx.doi.org/10.1016/j.mssp.2021.106154.

[21] H. Wang, J. Gazquez, C. Frontera, M.F. Chisholm, A. Pomar, B. Martinez, N. Mestres, Spontaneous cationic ordering in chemical-solution-grown La_2CoMnO_6 double perovskite thin films, NPG Asia Mater. 11 (2019) http://dx.doi.org/10.1038/s41427-019-0144-8.

[22] P. Paturi, H. Huhtinen, V. Paasonen, I. Angervo, Aqueous solutions, methods of manufacturing the same and uses thereof, Patent FI20225600 (30.6.2022), 2022.

[23] M. Matzapetakis, C.P. Raptopoulou, A. Tsohos, V. Papaefthymiou, A. Salifoglou, Synthesis, spectroscopic and structural characterization of the first mononuclear, water soluble iron-citrate complex, $(NH_4)_5Fe(C_6H_4O_7)_2 \cdot 2H_2O$, J. Am. Chem. Soc. 120 (1998) 13266, http://dx.doi.org/10.1021/ja9807035.

[24] D. Weber, R. Vőfély, Y. Chen, Y. Mourzina, U. Poppe, Variable resistor made by repeated steps of epitaxial deposition and lithographic structuring of oxide layers by using wet chemical etchants, Thin Solid Films 533 (2013) 43–47, http://dx.doi.org/10.1016/j.tsf.2012.11.118.

[25] B. Sarkar, R. Nag, S. Pal, Study of magnetic properties with temperature and field variation of electron doped $Ca_{0.85}Gd_{0.15}Mno_3$, Phys. B Cond. Matter 570 (2019) 224, http://dx.doi.org/10.1016/j.physb.2019.06.030.

[26] A. Beiranvand, M.O. Liedke, C. Haalisto, V. Lähteenlahti, A. Schulman, S. Granroth, H. Palonen, M. Butterling, A. Wagner, H. Huhtinen, P. Paturi, Tuned AFM-FM coupling by the formation of vacancy complex in $Gd_{0.6}Ca_{0.4}MnO_3$ thin film lattice, J. Phys.: Condens. Matter. 33 (2021) 255803, http://dx.doi.org/10.1088/1361-648x/abf9ba.

[27] J. Wu, C. Leighton, Glassy ferromagnetism and magnetic phase separation in $La_{1-x}Sr_xCoO_3$, Phys. Rev. B 67 (2003) 174408, http://dx.doi.org/10.1103/physrevb.67.174408.

[28] D.N.H. Nam, K. Jonason, P. Nordblad, N.V. Khiem, N.X. Phuc, Coexistence of ferromagnetic and glassy behaviour in the $La_{0.5}Sr_{0.5}CoO_3$ perovskite compound, Phys. Rev. B 59 (1999) 4189, http://dx.doi.org/10.1109/intmag.1999.837953.

[29] W. Boujelben, A. Cheikh-Rouhou, J. Pierre, J. Joubert, Effect of quenching on magnetic properties of polycrystalline $Pr_{0.5}Sr_{0.5}MnO_3$ perovskite manganite, J. Alloys Compd. 314 (2001) 15–21, http://dx.doi.org/10.1016/s0925-8388(00)01230-5.

[30] D. Krishna, Y.K. Lakshmi, B. Sreedhar, P.V. Reddy, Magnetic transport behavior of nanocrystalline $Nd_{0.67}A_{0.33}MnO_3$ (A=Ca, Sr, Pb and Ba), J. Solid State Sci. 11 (2009) 1312, http://dx.doi.org/10.1016/j.solidstatesciences.2009.04.002.

[31] A. Beiranvand, J. Tikkanen, H. Huhtinen, P. Paturi, Electronic and magnetic phase diagram of polycrystalline $Gd_{1-x}Ca_xMnO_3$ manganites, J. Alloy Compd. 720 (2017) 126–130, http://dx.doi.org/10.1016/j.jallcom.2017.05.231.

[32] S. Asanuma, H. Akoh, H. Yamada, A. Sawa, Relationship between resistive switching characteristics and band diagrams of Ti/ $Pr_{1-x}Ca_xMnO_3$ junctions, Phys. Rev. B 80 (2009) 235113, http://dx.doi.org/10.1103/physrevb.80.235113.

[33] M.J. Rozenberg, M.J. Sánchez, R. Weht, C. Acha, F. Gomez-Marlasca, P. Levy, Mechanism for bipolar resistive switching in transition-metal oxides, Phys. Rev. B 81 (2010) 115101, http://dx.doi.org/10.1103/physrevb.81.115101.

[34] Y.B. Nian, J. Strozier, N.J. Wu, X. Chen, A. Ignatiev, Evidence for an oxygen diffusion model for the electric pulse induced resistance change effect in transition-metal oxides, Phys. Rev. Lett. 98 (2007) 146403, http://dx.doi.org/10.1103/physrevlett.98.146403.

[35] T. Kramer, M. Scherff, D. Mierwaldt, J. Hoffmann, C. Jooss, Role of oxygen vacancies for resistive switching in noble metal sandwiched $Pr_{0.67}Ca_{0.33}Mno_{3-\delta}$, Appl. Phys. Lett. 110 (2017) 243502, http://dx.doi.org/10.1063/1.4985645.

[36] Z. Liao, P. Gao, X.B.D. Chen, J. Zhang, Evidence for electric-field-driven migration and diffusion of oxygen vacancies in $Pr_{0.7}Ca_{0.3}MnO_3$, J. Appl. Phys. 111 (2012) 114506, http://dx.doi.org/10.1063/1.4724333.

[37] A. Herpers, C. Lenser, C. Park, F. Offi, F. Borgatti, G. Panaccione, S. Menzel, R. Waser, R. Dittmann, Spectroscopic proof of the correlation between redox-state and charge-carrier transport at the interface of resistively switching Ti/PCMO devices, Adv. Mater. 26 (2014) 2730, http://dx.doi.org/10.1002/adma.201304054.